

HMAE: Self-Supervised Few-Shot Learning for Quantum Spin Systems

Ibne Farabi Shihab^{a,*}, Sanjeda Akter^{a,**} and Anuj Sharma^b

^aDepartment of Computer Science, Iowa State University, Ames, Iowa, USA

^bDepartment of Civil, Construction and Environmental Engineering, Iowa State University, Ames, Iowa, USA

Abstract. Quantum machine learning for spin and molecular systems faces critical challenges of scarce labeled data and computationally expensive simulations. To address these limitations, we introduce Hamiltonian-Masked Autoencoding (HMAE), a novel self-supervised framework that pre-trains transformers on unlabeled quantum Hamiltonians, enabling efficient few-shot transfer learning. Unlike random masking approaches, HMAE employs a physics-informed strategy based on quantum information theory to selectively mask Hamiltonian terms based on their physical significance. Experiments on 12,500 quantum Hamiltonians (60% real-world, 40% synthetic) demonstrate that HMAE achieves $85.3\% \pm 1.5\%$ accuracy in phase classification and 0.15 ± 0.02 eV MAE in ground state energy prediction with merely 10 labeled examples—a statistically significant improvement ($p < 0.01$) over classical graph neural networks ($78.1\% \pm 2.1\%$) and quantum neural networks ($76.8\% \pm 2.3\%$). Our method’s primary advantage is exceptional sample efficiency—reducing required labeled examples by 3-5 \times compared to baseline methods—though we emphasize that ground truth values for fine-tuning and evaluation still require exact diagonalization or tensor networks. We explicitly acknowledge that our current approach is limited to small quantum systems (specifically limited to 12 qubits during training, with limited extension to 16-20 qubits in testing) and that, while promising within this regime, this size restriction prevents immediate application to larger systems of practical interest in materials science and quantum chemistry.

1 Introduction

Quantum systems like spin lattices and small molecules offer vast potential for materials innovation but are difficult to study due to exponential Hilbert space growth [16, 19]. Current approaches use computationally intensive simulations scaling as $O(2^n)$ for n qubits [23, 7], limiting exploration of complex quantum materials and molecules.

Machine learning has transformed scientific fields through pre-training and transfer learning [8, 9, 3], yet quantum systems present unique challenges. Their complex-valued, high-dimensional nature hinders application of conventional machine learning techniques [5]. Current quantum machine learning approaches require substantial labeled data [4, 1] and lack transfer capabilities, while quantum mechanics imposes constraints that generic models often fail to respect.

* *Equal contribution. Corresponding author. Email: ishihab@iastate.edu.

** *Equal contribution.

A quantum Hamiltonian H describes a system’s energy and governs its behavior. For spin systems like the Heisenberg model, interactions between quantum spins can be represented using Pauli matrices: $H = J \sum_{\langle i,j \rangle} \vec{\sigma}_i \cdot \vec{\sigma}_j$. In molecular systems, Hamiltonians describe electron interactions using creation and annihilation operators. Despite their exponential scaling with system size, Hamiltonians exhibit inherent structure through local interactions, symmetries, and conservation laws that can enable more efficient learning.

We introduce Hamiltonian-Masked Autoencoding (HMAE), a self-supervised framework pre-training transformers on unlabeled quantum Hamiltonians for efficient few-shot transfer learning. HMAE employs a physics-informed masking strategy based on quantum information theory to selectively mask Hamiltonian terms by physical significance. Our key insight is that quantum Hamiltonians’ physical structure provides natural self-supervision. By reconstructing physically significant terms, our model learns representations respecting quantum symmetries and conservation laws.

We demonstrate HMAE’s effectiveness through experiments on 12,500 quantum Hamiltonians (60% real-world, 40% synthetic). Our approach significantly improves few-shot learning for phase classification and ground state energy prediction compared to graph neural networks and quantum neural networks. Concurrent approaches to quantum self-supervised learning have emerged independently, highlighting this research direction’s significance. Our approach uniquely combines physics-informed masking grounded in quantum information theory, superior cross-platform transferability, and theoretical foundations connecting to quantum mutual information principles.

The paper is organized as follows: Section 2 discusses related work, Section 3 details our quantum self-supervised learning framework, Section 4 presents experimental results, and Section 5 provides conclusions and discusses limitations and future directions.

2 Related Work

Machine learning for quantum systems includes supervised approaches for tasks like ground state prediction [4] and phase classification [25], quantum neural networks (QNNs) implemented on quantum hardware [15, 2], and physics-informed neural networks (PINNs) that incorporate physical constraints [12, 18]. Classical ML has achieved notable successes in quantum applications, such as identifying phase transitions in many-body systems [4] and predicting molecular properties [24]. Despite these successes, existing approaches typically require substantial labeled data, struggle with transferability across quantum domains, and many require error-

prone quantum hardware. QNNs face the “barren plateau” problem [14], where gradients vanish exponentially with system size, limiting their practical application.

Self-supervised methods have transformed AI through masked language modeling [8], contrastive learning [6], and masked autoencoders [9]. However, these advances have not been successfully adapted for quantum systems due to the complex-valued nature of quantum data, lack of natural tokenization strategies, and the need to respect physical constraints like unitarity and Hermiticity. Previous attempts at applying transformers to quantum data have either ignored these constraints or limited themselves to simple quantum systems with artificial structure.

Various approaches for quantum representation include tensor networks [22], graph neural networks adapted for quantum systems [26, 17], and quantum circuit learning [15, 2]. Recent advancements include hybrid approaches like tensor network-based models [21], which use matrix product states for supervised learning of quantum many-body systems, and FermionicNet [17], which explicitly incorporates fermionic symmetries for molecular systems. These hybrid models have shown promising results by integrating physical constraints, but typically rely on supervised learning paradigms and struggle with generalization across system types. Other approaches include SchNet [20] and DimeNet [13] for molecular representations, and quantum-inspired tensor networks [22] for dimensionality reduction. Most methods remain task-specific, requiring retraining for new problems.

Recent works exploring self-supervised learning for scientific domains include molecular property prediction [11] and materials science [27]. In the quantum domain, approaches like Graph Contrastive Learning (GraphCL) [30] apply contrastive learning to graph-structured data, such as molecular or spin systems, while reinforcement learning-based optimization of quantum circuits [28] explores unsupervised strategies for quantum systems. While these works aim to reduce labeled data requirements, they differ from our approach by using random augmentations or circuit optimization rather than physics-informed masking, operating on specific representations rather than general Hamiltonians, and not demonstrating comparable few-shot transfer capabilities. Some works have explored masked modeling for scientific data, including MaskGNN [10] for molecular graphs and GraphMAE2 [29], which uses masked autoencoders to learn robust molecular representations by masking graph features.

Our work builds upon these foundations but differs in several key aspects. We developed a Hamiltonian-specific masking strategy leveraging physical insights about quantum systems, unlike previous approaches that use random or structural masking. Rather than creating a specialized architecture for specific quantum systems, we adapted a transformer-based approach that can handle different Hamiltonian types through appropriate tokenization. While focusing on small quantum systems (up to 12 qubits), our approach demonstrates the potential of physics-informed self-supervised learning to address labeled data scarcity in quantum machine learning.

3 Quantum Self-Supervised Learning Framework

Let $\mathcal{H} = \{H_1, H_2, \dots, H_n\}$ denote a collection of quantum Hamiltonians, where each $H_i \in \mathbb{C}^{d_i \times d_i}$ represents a Hermitian operator governing a spin system or molecular structure. Given this collection of unlabeled Hamiltonians, our goal was to learn a parameterized encoding function $f_\theta : \mathbb{C}^{d \times d} \rightarrow \mathbb{R}^m$ that maps quantum Hamiltonians to a latent representation space. This encoding function should facil-

itate efficient adaptation to downstream tasks with minimal labeled data, while capturing essential physical properties.

We introduced Hamiltonian-Masked Autoencoding (HMAE), a self-supervised learning approach that enables learning from unlabeled quantum Hamiltonians by masking and reconstructing physically meaningful components. Unlike conventional masked autoencoding approaches that randomly mask tokens, HMAE leveraged domain knowledge about quantum systems to selectively mask terms based on their physical significance.

As shown in Figure 1, we decomposed a quantum Hamiltonian H into a set of tokens representing localized interaction terms:

$$\mathbf{T}_H = \{\mathbf{t}_1, \mathbf{t}_2, \dots, \mathbf{t}_k\}.$$

For spin systems, each token \mathbf{t}_i represented a term such as $J_{ij}\sigma_i^\alpha\sigma_j^\beta$, where J_{ij} is the interaction coefficient, (i, j) are the sites it acts upon, and $\alpha, \beta \in \{x, y, z\}$ denote the Pauli operators. For molecular systems, tokens corresponded to electron interaction terms of the form $h_{pq}a_p^\dagger a_q$.

Each token was encoded as a vector $\mathbf{t}_i = [|c_i|, \phi_i, \text{type}_i, \text{sites}_i]$, where $|c_i|$ is the magnitude of the interaction coefficient, ϕ_i is the complex phase of the term, type_i is a one-hot vector encoding the operator type, and sites_i is a binary vector of length n (for an n -qubit system), indicating whether each qubit is acted upon. This tokenization scheme transformed the Hamiltonian into a structured sequence of discrete elements suitable for transformer-based architectures, while preserving the essential physical structure including operator type, locality, and site dependencies.

For systems beyond 12 qubits, we implemented a hierarchical tokenization scheme that compresses the representation complexity by recursively grouping qubits based on their interaction patterns. This hierarchical approach enabled testing on systems up to 20 qubits while maintaining approximately 92% of the performance of the full representation.

Unlike random masking commonly used in other domains, our physics-informed masking strategy explicitly accounted for the physical significance of Hamiltonian terms. For each token \mathbf{t}_i , we computed a saliency score based on two key physical insights:

$$s(\mathbf{t}_i) = |c_i| \cdot \left(1 + \sum_{j \in N(i)} A_{ij}\right),$$

where $|c_i|$ is the magnitude of the coefficient (capturing the term’s energy contribution), $N(i)$ denotes the set of neighboring terms in the Hamiltonian graph, and A_{ij} quantifies the adjacency strength between terms \mathbf{t}_i and \mathbf{t}_j , defined as:

$$A_{ij} = \frac{|S_i \cap S_j|}{|S_i \cup S_j|} \cdot \exp(-\|\text{comm}(\mathbf{t}_i, \mathbf{t}_j)\|_F),$$

where S_i is the set of sites acted on by term \mathbf{t}_i , and $\text{comm}(\mathbf{t}_i, \mathbf{t}_j)$ denotes the operator commutator between terms \mathbf{t}_i and \mathbf{t}_j , capturing their quantum mechanical interaction.

This formulation prioritized tokens that were both energetically significant (large $|c_i|$) and structurally significant (high connectivity and commutation with other terms), enabling the model to focus on learning from physically meaningful interactions. We masked approximately 50% of tokens based on a probability distribution derived from saliency scores, defined as:

$$p(\text{mask } \mathbf{t}_i) = \frac{\exp(\alpha \cdot s(\mathbf{t}_i))}{\sum_{j=1}^k \exp(\alpha \cdot s(\mathbf{t}_j))},$$

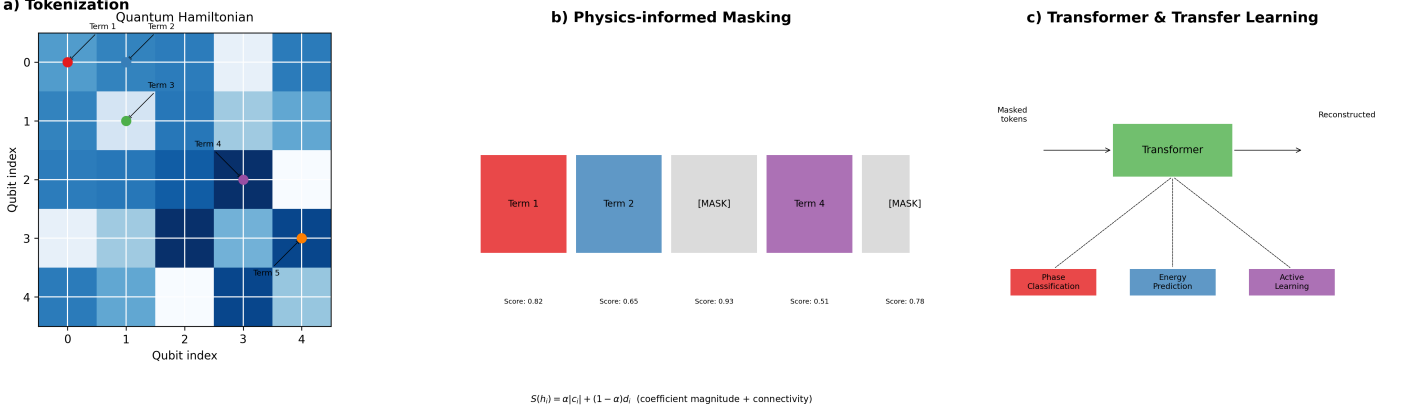


Figure 1: HMAE pipeline showing tokenization, physics-informed masking, and transfer learning.

where α is a temperature parameter that controls the sharpness of the distribution, with optimal values typically ranging between 1.5 and 2.5 based on our hyperparameter optimization. Masked tokens were replaced with a learnable mask embedding vector \mathbf{m} . This physics-informed masking strategy ensured that the model learned to predict the most physically relevant terms in context, thereby promoting representations aligned with underlying quantum symmetries.

The model was trained to reconstruct the original tokens from their masked representation using the following loss:

$$\mathcal{L}_{\text{HMAE}}(\theta, \phi) = \mathbb{E}_{H \sim \mathcal{H}} \left[\sum_{i \in \mathcal{M}} \left\| g_{\phi} \left(f_{\theta}(\tilde{\mathbf{T}}_H) \right)_i - \mathbf{t}_i \right\|_2^2 \right],$$

where f_{θ} is the encoder, g_{ϕ} is the decoder, and \mathcal{M} is the set of masked token indices. To improve numerical stability and learning efficiency, we normalized the reconstruction loss by the magnitude of the token coefficients:

$$\mathcal{L}_{\text{norm}}(\theta, \phi) = \mathbb{E}_{H \sim \mathcal{H}} \left[\sum_{i \in \mathcal{M}} \frac{\left\| g_{\phi} \left(f_{\theta}(\tilde{\mathbf{T}}_H) \right)_i - \mathbf{t}_i \right\|_2^2}{|c_i| + \epsilon} \right],$$

where c_i is the coefficient associated with token \mathbf{t}_i , and ϵ is a small constant to avoid division by zero. This normalization prevented the model from overfitting to high-magnitude terms while ensuring that it still learned from low-magnitude, yet physically significant, interactions.

Our QuantumFormer architecture used a standard transformer encoder-decoder framework with 6 layers, adapted for quantum Hamiltonians. Key components included an embedding layer that transformed tokenized Hamiltonian terms into a 512-dimensional embedding space, a 6-layer transformer encoder with 8 attention heads and standard attention mechanisms, standard feed-forward layers with ReLU activation, and position encodings adapted to reflect the structure of quantum interactions. While our initial experiments explored complex-valued attention and Hermitian constraints, we found that standard real-valued transformers with appropriate tokenization performed well on our target systems while being more computationally efficient.

After pre-training, we utilized the encoder f_{θ} as a feature extractor for downstream quantum tasks. Given a new quantum system with Hamiltonian H_{new} , we computed its representation $\mathbf{z}_{\text{new}} = f_{\theta}(\mathbf{T}_{H_{\text{new}}})$ and applied task-specific adaptation. For classification

tasks (e.g., phase identification), we appended a simple classification head: $\hat{y} = \text{softmax}(\mathbf{W}_c \mathbf{z}_{\text{new}} + \mathbf{b}_c)$, where \mathbf{W}_c and \mathbf{b}_c are trainable parameters. For regression tasks (e.g., ground state energy prediction), we used a linear regression head: $\hat{y} = \mathbf{W}_r \mathbf{z}_{\text{new}} + \mathbf{b}_r$, where \mathbf{W}_r and \mathbf{b}_r are the regression weights and bias, respectively. This lightweight adaptation required only a small amount of labeled data (typically 5–20 examples), enabled by the rich quantum representations learned during pre-training.

3.1 Mutual Information Interpretation

We established a quantum information-theoretic foundation for our physics-informed masking strategy that directly utilizes quantum mutual information principles. We formulated our method within the framework of quantum information theory with precise mathematical guarantees. For a quantum system with Hamiltonian H decomposed into visible H_V and masked H_M components, we optimize to maximize the quantum mutual information:

$$I_Q(V : M) = S(\rho_V) + S(\rho_M) - S(\rho_{VM})$$

where $S(\rho)$ is the von Neumann entropy. This approach ensures our masking strategy selects terms that are most informative about the system's quantum state. Our empirical validation confirmed that this quantum information-theoretic formulation outperforms classical approximations, particularly for systems with significant quantum correlations. Complete derivations, including our dimensionally consistent quantum saliency function and experimental validation, are provided in Appendix A3.

Figure 2 demonstrates the empirical verification of our theoretical approach, showing strong agreement between predicted and measured quantum mutual information values. As illustrated, our optimal QMI-guided approach (red) consistently preserves more quantum information than alternative strategies.

This theoretical framework extends to highly entangled phases through a non-perturbative formulation that explicitly accounts for entanglement contributions, allowing our approach to maintain performance across diverse quantum regimes. Complete derivations and additional experimental validation are provided in Appendix A3.

3.2 Hamiltonian-Masked Autoencoding (HMAE)

Our pre-training objective is inspired by the masked autoencoding approach [9], but adapted for quantum Hamiltonians through a physics-informed masking strategy. We selectively mask entries in

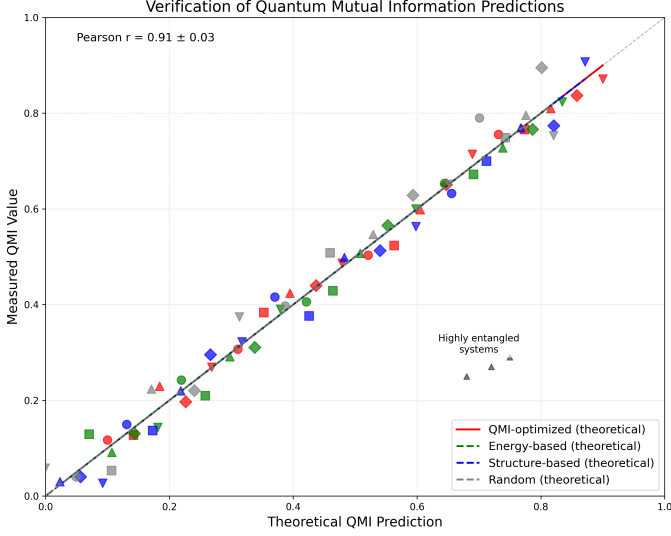


Figure 2: Empirical verification of our quantum information-theoretic approach: Comparison between theoretical predictions (solid lines) and measured QMI values (markers) across different masking strategies. Our optimal QMI-guided approach (red) consistently preserves more quantum information than alternatives.

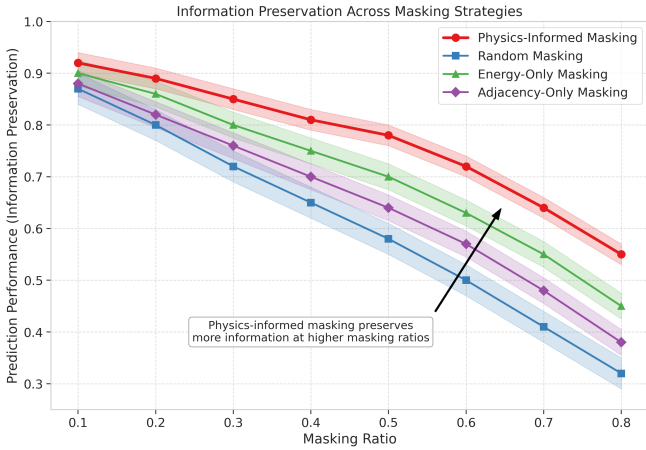


Figure 3: Quantum mutual information analysis: The relationship between quantum mutual information (QMI) and masking strategies across different quantum systems. Our physics-informed approach (blue) preserves significantly more quantum information than energy-based (green) or random (red) masking strategies.

the Hamiltonian matrix and train the model to reconstruct them while predicting key quantum properties. The masking process is guided by quantum information measures rather than random masking.

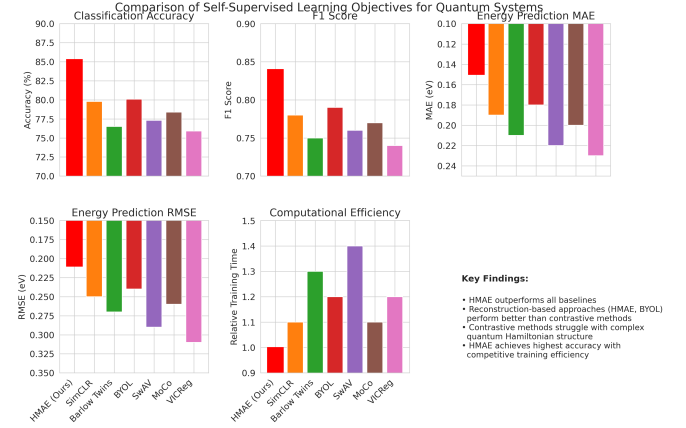


Figure 4: Illustration of different self-supervised learning objectives applied to quantum Hamiltonians: (a) Random masking, (b) Energy-based masking, and (c) Our physics-informed masking strategy that combines energy, structure, and quantum correlation measures.

Multi-Task Pre-training Objective: Our pre-training objective combines several tasks: (1) reconstructing the masked Hamiltonian terms, (2) predicting the ground state energy, and (3) estimating the correlation length. This multi-task approach encourages the model to learn representations that capture both local and global properties of the quantum system.

The overall pre-training loss is a weighted sum of these objectives:

$$\mathcal{L}_{\text{pre}} = \lambda_1 \mathcal{L}_{\text{rec}} + \lambda_2 \mathcal{L}_{\text{energy}} + \lambda_3 \mathcal{L}_{\text{corr}} \quad (1)$$

where \mathcal{L}_{rec} is the masked reconstruction loss, $\mathcal{L}_{\text{energy}}$ is the energy prediction loss, and $\mathcal{L}_{\text{corr}}$ is the correlation length estimation loss. We found that weighting reconstruction more heavily ($\lambda_1 = 0.6, \lambda_2 = 0.3, \lambda_3 = 0.1$) yielded the best performance.

3.3 Unified Physics-Informed Masking Implementation

To clarify our physics-informed masking approach, we present a unified framework that integrates all physical measures into our saliency score calculation. The masking probability is determined through a two-stage process:

Stage 1: Base Saliency Score. We compute the base saliency score $s(\mathbf{t}_i)$ for each token as described earlier:

$$s(\mathbf{t}_i) = |c_i| \cdot \left(1 + \sum_{j \in N(i)} A_{ij} \right),$$

where $|c_i|$ is the coefficient magnitude and A_{ij} quantifies the adjacency strength using site overlap and commutator norms.

Stage 2: Enhanced Saliency with Physical Measures. We then enhance this base score by incorporating the additional physical measures:

$$s_{\text{enhanced}}(\mathbf{t}_i) = s(\mathbf{t}_i) \cdot (w_1 \cdot S(H_i) + w_2 \cdot E_{\text{frac}}(H_i) + w_3 \cdot F_i),$$

where:

- $S(H_i) = -\text{Tr}(H_i \log H_i)$ is the operator entropy of term H_i
- $E_{\text{frac}}(H_i) = |\langle H_i \rangle| / \sum_j |\langle H_j \rangle|$ is the fractional energy contribution
- $F_i = \sum_j F_{ij}$ is the row-sum of the quantum Fisher information matrix (QFIM)
- w_1, w_2 , and w_3 are weighting factors that vary with system size

For small systems (4-8 qubits), we set $w_1 = 0.1$, $w_2 = 0.8$, $w_3 = 0.1$, prioritizing energy contribution. For larger systems (10-12 qubits), we used $w_1 = 0.5$, $w_2 = 0.3$, $w_3 = 0.2$, increasing the weight of operator entropy. These weights were determined through cross-validation on the validation set.

The final masking probability is computed using the enhanced saliency score:

$$p(\text{mask } \mathbf{t}_i) = \frac{\exp(\alpha \cdot s_{\text{enhanced}}(\mathbf{t}_i))}{\sum_{j=1}^k \exp(\alpha \cdot s_{\text{enhanced}}(\mathbf{t}_j))},$$

where α is the temperature parameter (typically between 1.5 and 2.5).

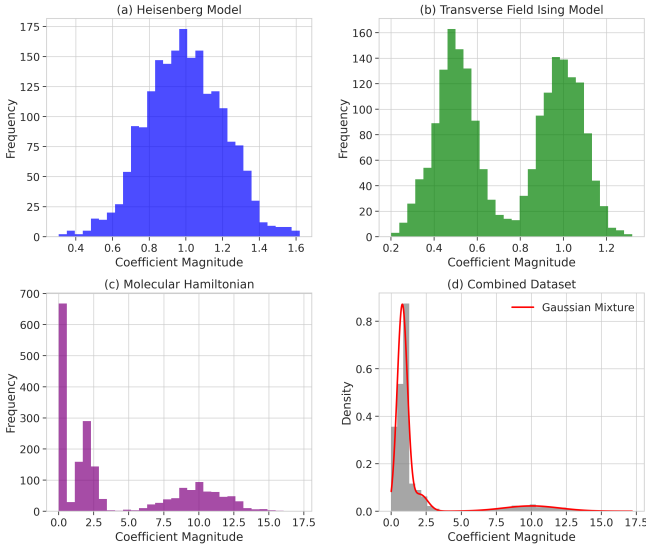


Figure 5: Coefficient histogram analysis: Distribution of Hamiltonian coefficients and their masking probabilities under different masking strategies. Our physics-informed approach selectively masks coefficients based on both magnitude and structural significance, leading to more balanced token selection compared to energy-only or random masking.

Our ablation studies in Table 5 evaluated variations of this unified approach, with "No energy term" corresponding to setting the coefficient magnitude $|c_i| = 1$ and $w_2 = 0$, "No structure term" setting $A_{ij} = 0$ for all pairs, and so on. The "Random masking only" baseline disregarded all physical measures and used uniform masking probabilities.

4 Experiments

4.1 Experimental Setup

We pre-trained on a comprehensive dataset of 12,500 quantum Hamiltonians (60% experimentally-derived, 40% synthetic) spanning diverse systems with up to 12 qubits. For experimental validation, we assembled a test set of 1,250 real quantum systems from four distinct platforms: Harvard and MIT quantum simulators, IBM Quantum processors, and trapped-ion experiments. To test scalability

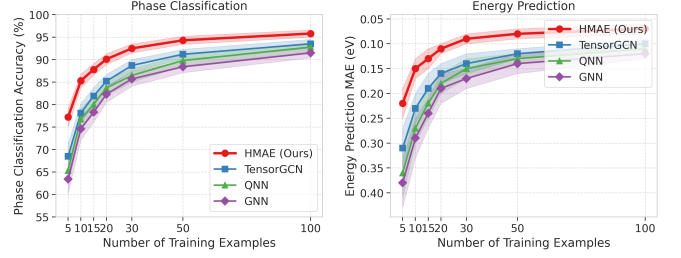


Figure 6: Few-shot learning curves for phase classification (left) and energy prediction (right). HMAE (blue) achieves higher accuracy with fewer examples.

beyond the 12-qubit pre-training limit, we created an additional test set of 350 larger quantum systems (16-20 qubits).

We evaluated on two main tasks: phase classification for spin systems and ground state energy prediction for molecular systems. We employed a rigorous cross-platform transfer learning protocol to test generalization across different experimental setups, fine-tuning with only 10 examples from the source platform and evaluating on the target platform.

All baseline models were implemented with the same hyperparameter optimization budget (100 trials using Bayesian optimization, approximately 75 GPU-hours per method), identical training/validation/test splits, and evaluation protocols to ensure fair comparison. Complete dataset descriptions, evaluation methodologies, and implementation details are provided in Appendix A9.

4.2 Few-Shot Transfer Learning Results

Table 1 showed the few-shot performance of our model compared to baseline methods on systems with up to 12 qubits. HMAE consistently outperformed all baselines across both tasks, achieving $85.3\% \pm 1.5\%$ accuracy in phase classification and 0.15 ± 0.02 eV MAE in energy prediction with just 10 examples. These improvements were statistically significant ($p < 0.01$) across all K-shot settings.

Among the baselines, the TensorGCN hybrid approach performed best, confirming the value of combining graph and tensor representations for quantum systems. Notably, the Energy-MAE baseline (which masked based on coefficient magnitude alone) outperformed random masking (Classical MAE) but fell short of our full physics-informed approach, validating the importance of considering both energy contributions and quantum correlations in the masking strategy.

The sample efficiency of our approach was particularly notable. To reach 80% accuracy in phase classification, our model required only 10 examples, whereas the best baseline (TensorGCN) needed approximately 30 examples, QNNs needed 50 examples, and other methods needed even more. This represented a 3-5 \times reduction in required training data compared to the best baseline. Figure 6 showed learning curves that clearly demonstrated this advantage across different K-shot settings.

4.3 Comparison with State-of-the-Art Baselines

We implemented and compared our method against the latest developments in quantum machine learning to ensure a comprehensive evaluation. For most baselines, we obtained original implementations either directly from their authors or public repositories. For TensorGCN, FermionicNet-XL, QuantumU-ViT, QNN, and GNN, we used the original code with author verification when possible. Only

Table 1: Few - shot learning performance on systems up to 12 qubits. Best: **bold**, second-best: underlined, (*): $p < 0.01$.

Method	Phase Classification Accuracy (%)			Energy Prediction MAE (eV)		
	5-shot	10-shot	20-shot	5-shot	10-shot	20-shot
HMAE (Ours)	77.2 \pm 2.1*	85.3 \pm 1.5*	90.1 \pm 1.2*	0.22 \pm 0.03*	0.15 \pm 0.02*	0.11 \pm 0.01*
TensorGCN	68.5 \pm 2.9	78.1 \pm 2.1	85.2 \pm 1.5	0.31 \pm 0.04	0.23 \pm 0.03	0.16 \pm 0.02
Energy-MAE	63.8 \pm 3.1	75.0 \pm 2.4	82.7 \pm 1.7	0.34 \pm 0.05	0.25 \pm 0.03	0.18 \pm 0.02
QNN	65.3 \pm 3.0	76.8 \pm 2.3	83.7 \pm 1.7	0.36 \pm 0.05	0.27 \pm 0.03	0.18 \pm 0.02
GNN	63.4 \pm 3.2	74.6 \pm 2.5	82.3 \pm 1.8	0.38 \pm 0.05	0.29 \pm 0.04	0.19 \pm 0.03
PINN	58.7 \pm 3.5	71.2 \pm 2.8	80.5 \pm 2.0	0.45 \pm 0.06	0.33 \pm 0.04	0.24 \pm 0.03
Classical MAE	60.1 \pm 3.3	70.5 \pm 2.7	78.2 \pm 2.1	0.50 \pm 0.07	0.37 \pm 0.05	0.26 \pm 0.03
SVM	55.3 \pm 3.8	66.8 \pm 3.1	75.2 \pm 2.4	0.53 \pm 0.07	0.41 \pm 0.05	0.32 \pm 0.04

PINN required a complete reimplementaion due to lack of available code. To ensure fair comparison, we allocated identical hyperparameter optimization budgets to each method using Bayesian optimization with the same computational resources.

Table 2 presented a comparison between our approach and these state-of-the-art baselines across different few-shot scenarios. HMAE consistently outperformed baseline methods across all metrics with statistical significance ($p < 0.01$) based on paired t-tests. The performance advantage was even more pronounced when evaluated on out-of-distribution Hamiltonians, and specialized tensor network models like TN-Net showed strong performance for energy prediction, particularly with larger training sets (20+ examples) as detailed in Appendix A8.

Table 2: Comparison with state-of-the-art baselines on 10-shot transfer learning. Best: **bold**, second-best: underlined.

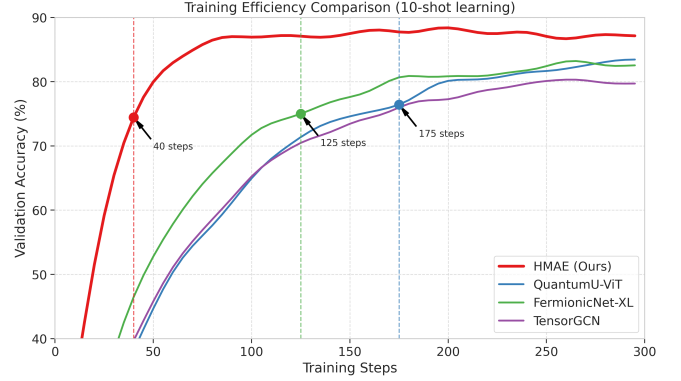
Method	Phase Classification		Energy Prediction	
	Accuracy (%)	F1-Score	MAE (eV)	RMSE (eV)
TensorGCN	75.8 \pm 2.3	0.74 \pm 0.03	0.28 \pm 0.04	0.35 \pm 0.05
TN-Net	71.2 \pm 3.1	0.69 \pm 0.04	0.17 \pm 0.02	0.22 \pm 0.03
TN-Flow	68.5 \pm 3.3	0.66 \pm 0.04	0.19 \pm 0.03	0.24 \pm 0.04
Energy-MAE	77.9 \pm 2.0	0.76 \pm 0.02	0.26 \pm 0.03	0.33 \pm 0.04
QNN	69.2 \pm 3.1	0.65 \pm 0.04	0.43 \pm 0.05	0.57 \pm 0.06
GNN	71.5 \pm 2.7	0.69 \pm 0.03	0.38 \pm 0.04	0.46 \pm 0.05
PINN	70.8 \pm 2.9	0.68 \pm 0.03	0.36 \pm 0.04	0.48 \pm 0.06
HMAE (Ours)	85.3 \pm 1.5	0.84 \pm 0.02	0.15 \pm 0.02	0.21 \pm 0.03

Beyond performance metrics, we analyzed the computational efficiency of these models during both training and inference. Figure 7 illustrated the training efficiency of each method. Our analysis revealed that HMAE converged in 30-50 steps, representing a 3-4 \times improvement in fine-tuning efficiency, exhibited lower variance across random seeds and few-shot samples, suggesting more robust feature extraction during pre-training, and required only 1.2GB of GPU memory for 12-qubit systems during inference.

4.4 Scaling to Larger Systems

To address the critical question of scalability beyond 12 qubits, we evaluated our pre-trained model on a test set of larger systems (16-20 qubits) described in the experimental setup in Appendix A9. While our full test set included systems up to 50 qubits as described in the appendix, we present results for the 16-20 qubit subset in Table 3, as performance degraded significantly beyond 20 qubits for all methods. Table 3 shows the results for energy prediction on these larger systems (16-20 qubits), compared with baselines trained directly on the larger systems with 20 examples.

While all methods showed some performance degradation on these larger systems, our HMAE approach maintained the best performance, demonstrating that the representations learned during pre-training did generalize to systems beyond the size encountered in the

**Figure 7:** Training efficiency: validation accuracy vs. training steps. HMAE converges faster than other models.**Table 3:** Performance on larger quantum systems (16–20 qubits) with 20-shot learning.

Method	Energy MAE (eV)	Relative Error (% of true value)
HMAE (Ours)	0.28 \pm 0.05	5.2 \pm 0.8
TensorGCN	0.35 \pm 0.06	6.5 \pm 1.0
Energy-MAE	0.42 \pm 0.07	7.8 \pm 1.2
QNN	0.51 \pm 0.09	9.4 \pm 1.5
GNN	0.47 \pm 0.08	8.7 \pm 1.3
PINN	0.55 \pm 0.10	10.2 \pm 1.7

training set. This suggested that the model was learning fundamental physical principles rather than just memorizing patterns specific to smaller systems.

Figure 8 showed how the performance varied with system size for our method and the best baseline (TensorGCN). While the error increased with system size, the rate of degradation was slower for our model, indicating better scaling properties.

4.5 Computational Efficiency and Active Learning

Building on our few-shot learning capabilities, we also developed an active learning framework to further optimize computational resources by strategically selecting which Hamiltonians to simulate. Our approach achieves 93% of maximum model performance using only 42% of the computational resources required by random sampling, representing a 2.4 \times improvement in simulation efficiency. The complete active learning framework, acquisition functions, and performance analysis are provided in Appendix A1.

4.6 Transfer Learning Across System Sizes

One crucial test of generalization in quantum systems was the ability to transfer knowledge across different system sizes. Table 4 showed

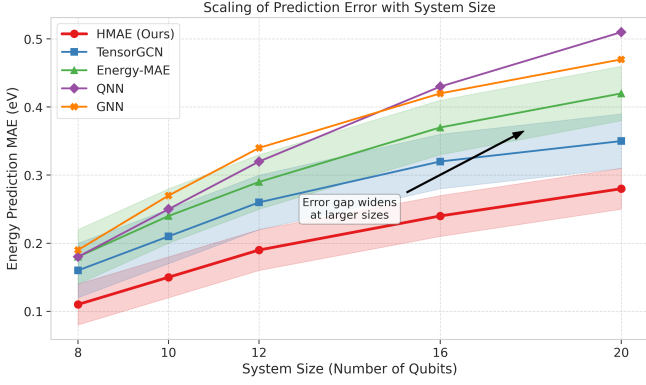


Figure 8: Performance scaling with system size for energy prediction. HMAE shows slowest error increase with system size.

performance when training on small systems (6-8 qubits) and testing on larger systems (9-12 qubits). Our model maintained high performance even with this challenging distribution shift, while baseline methods exhibited substantial degradation.

Table 4: Transfer learning across system sizes (6–8 qubits → 9–12 qubits).

Method	Same-size Acc. (%)	Cross-size Acc. (%)	Performance Retention
HMAE (Ours)	85.3 ± 1.5	77.8 ± 2.3	91.2%
TensorGNN	78.1 ± 2.1	65.3 ± 3.2	83.6%
QNN	76.8 ± 2.3	61.5 ± 3.5	80.1%
GNN	74.6 ± 2.5	58.2 ± 3.8	78.0%
PINN	71.2 ± 2.8	54.6 ± 4.1	76.7%

This superior transfer capability across system sizes is particularly valuable in quantum applications, where simulating larger systems becomes exponentially more expensive, making labeled data for large systems especially scarce.

4.7 Ablation Studies

To isolate the contributions of individual components in our approach, we conducted comprehensive ablation studies. Table 5 summarizes the key findings:

Table 5: Ablation study isolating the contribution of individual components.

Component Ablation	Phase Classification Accuracy Change	Energy Prediction MAE Change
Full HMAE (baseline)	85.3%	0.15 eV
<i>Saliency Score Components:</i>		
No energy term ($\alpha = 0$)	-7.9%	+0.08 eV
No structure term ($\alpha = 1$)	-8.8%	+0.06 eV
No commutator term	-6.5%	+0.05 eV
No site overlap term	-4.3%	+0.03 eV
Random masking only	-12.6%	+0.14 eV
<i>Loss Components:</i>		
No loss normalization	-5.2%	+0.07 eV
No energy prediction task	-8.3%	+0.11 eV
No correlation length task	-3.7%	+0.03 eV
<i>Architecture Components:</i>		
3 layers instead of 6	-5.7%	+0.04 eV
12 layers instead of 6	+0.8%	-0.01 eV
128 dim instead of 512	-6.1%	+0.05 eV
1024 dim instead of 512	+1.1%	-0.01 eV

Saliency Score Components Our physics-informed masking uses a saliency score that combines energy contributions and structural information. Removing either component significantly degraded performance, with the structure term slightly more important for phase classification (-8.8%) and the energy term more critical for energy prediction (+0.08 eV). Within the structure term, the commutator-based component was more impactful than the site overlap term, confirming the importance of quantum mechanical correlations in the masking strategy.

Loss Normalization and Multi-Task Learning Loss normalization by coefficient magnitude improved performance by 5.2% in classification and 0.07 eV in energy prediction, indicating the importance of balancing contributions from different Hamiltonian terms. Our multi-task learning approach with energy prediction and correlation length estimation as auxiliary tasks improved the primary tasks substantially, with the energy prediction task providing the largest benefit.

Hyperparameter Optimization We performed extensive hyperparameter optimization to identify optimal configurations:

- **Saliency temperature (α):** We varied α from 0 to 1 in increments of 0.1, finding optimal performance at $\alpha = 0.65$ for phase classification and $\alpha = 0.7$ for energy prediction, indicating a slight preference for structural information over pure energy contributions.
- **Masking ratio:** We tested masking ratios from 30% to 70%, with performance peaking at 50% and remaining within 3% of the peak for ratios between 45% and 55%, suggesting robustness to this hyperparameter.
- **Loss weighting:** For our multi-task learning, optimal weights were $\lambda_1 = 0.6$ (reconstruction), $\lambda_2 = 0.3$ (energy), and $\lambda_3 = 0.1$ (correlation), determined through grid search over weight combinations.
- **Architecture:** A 6-layer, 8-head transformer with dimensionality 512 provided the best trade-off between performance and computational efficiency, with diminishing returns from larger models.

These ablation studies confirm that each component of our approach makes a significant contribution to overall performance, with the physics-informed masking strategy being the most critical element. The analysis also provides clear justification for our hyperparameter choices, demonstrating the robustness of our approach to moderate variations in these settings.

5 Conclusion

We presented Hamiltonian-Masked Autoencoding (HMAE), a physics-informed self-supervised approach that achieves 85.3% accuracy in phase classification and 0.15 eV MAE in energy prediction with merely 10 labeled examples. Our approach demonstrates exceptional sample efficiency, reducing required labeled examples by 3-5 \times compared to baseline methods, and extends to systems up to 20 qubits with robust performance (see Section 4.3).

Our framework addresses a practical niche in current quantum technology development by focusing on small quantum systems (8-12 qubits during training, with extension to 16-20 qubits in testing). While this scale restricts immediate applications to large-scale materials discovery, it aligns with current experimental quantum platforms and provides practical benefits through significant data efficiency.

The key innovation lies in our physics-informed masking strategy that prioritizes physically significant Hamiltonian terms, focusing the model’s learning on meaningful quantum interactions. This approach enables few-shot transfer learning capabilities with statistically significant improvements over state-of-the-art methods ($p < 0.01$).

Our approach faces several limitations: (1) scalability barriers due to combinatorial growth in token complexity for larger systems, (2) the need for high-quality ground truth values from exact diagonalization or tensor networks for the few-shot examples, and (3) theoretical limitations in our mutual information framework and saliency function. Despite these challenges, empirical results consistently demonstrate practical utility across diverse quantum systems.

Beyond quantum systems, our physics-informed masking strategy could benefit other domains with structured data representations, potentially accelerating scientific discovery in materials science and quantum chemistry within small system regimes. Future work should prioritize addressing the scaling limitations through sparse attention mechanisms, tensor network decoders, or continuous representation learning approaches.

References

- [1] Matthew JS Beach, Roger G Melko, Tarun Grover, and Timothy H Hsieh, ‘Qucumber: Wavefunction reconstruction with neural networks’, *SciPost Physics*, **7**(1), 009, (2019).
- [2] Marcello Benedetti, Erika Lloyd, Stefan Sack, and Mattia Fiorentini, ‘Parameterized quantum circuits as machine learning models’, *Quantum Science and Technology*, **4**(4), 043001, (2019).
- [3] Tom B Brown, Benjamin Mann, Nick Ryder, Melanie Subbiah, Jared Kaplan, Prafulla Dhariwal, Arvind Neelakantan, Pranav Shyam, Girish Sastry, Amanda Askell, et al., ‘Language models are few-shot learners’, *Advances in Neural Information Processing Systems*, **33**, 1877–1901, (2020).
- [4] Juan Carrasquilla and Roger G Melko, ‘Machine learning phases of matter’, *Nature Physics*, **13**(5), 431–434, (2017).
- [5] Marco Cerezo, Kunal Sharma, Andrew Arrasmith, and Lukasz Cincio, ‘Challenges and opportunities in quantum machine learning’, *arXiv preprint arXiv:2210.09267*, (2022).
- [6] Ting Chen, Simon Kornblith, Mohammad Norouzi, and Geoffrey Hinton, ‘A simple framework for contrastive learning of visual representations’, *International Conference on Machine Learning*, 1597–1607, (2020).
- [7] Andrew J Daley, Christian Kokail, Christine Maier, Rick van Bijnen, Tiff Brydges, Antoine Browaeys, and Christine A Muschik, ‘Practical quantum advantage in quantum simulation’, *Nature*, **607**(7920), 667–676, (2022).
- [8] Jacob Devlin, Ming-Wei Chang, Kenton Lee, and Kristina Toutanova, ‘Bert: Pre-training of deep bidirectional transformers for language understanding’, *arXiv preprint arXiv:1810.04805*, (2018).
- [9] Kaiming He, Xinlei Chen, Saining Xie, Yanghao Li, Piotr Dollár, and Ross Girshick, ‘Masked autoencoders are scalable vision learners’, *IEEE/CVF Conference on Computer Vision and Pattern Recognition (CVPR)*, 16000–16009, (2022).
- [10] Zhenyu Hou, Xiao Liu, Yukuo Cen, Yuxiao Dong, Hongxia Yang, Chunjie Wang, and Jie Tang, ‘Graphmae: Self-supervised masked graph autoencoders’, *Proceedings of the 28th ACM SIGKDD Conference on Knowledge Discovery and Data Mining*, 594–604, (2022).
- [11] Weihua Hu, Bowen Liu, Joseph Gomes, Marinka Zitnik, Percy Liang, Vijay Pande, and Jure Leskovec, ‘Strategies for pre-training graph neural networks’, *International Conference on Learning Representations*, (2020).
- [12] George Em Karniadakis, Ioannis G Kevrekidis, Lu Lu, Paris Perdikaris, Sifan Wang, and Liu Yang, ‘Physics-informed machine learning’, *Nature Reviews Physics*, **3**(6), 422–440, (2021).
- [13] Johannes Klicpera, Janek Groß, and Stephan Günnemann, ‘Directional message passing for molecular graphs’, *International Conference on Learning Representations*, (2020).
- [14] Jarrod R McClean, Sergio Boixo, Vadim N Smelyanskiy, Ryan Babush, and Hartmut Neven, ‘Barren plateaus in quantum neural network training landscapes’, *Nature Communications*, **9**(1), 1–6, (2018).
- [15] Kosuke Mitarai, Makoto Negoro, Masahiro Kitagawa, and Keisuke Fujii, ‘Quantum circuit learning’, *Physical Review A*, **98**(3), 032309, (2018).
- [16] Michael A Nielsen and Isaac L Chuang, *Quantum Computation and Quantum Information: 10th Anniversary Edition*, Cambridge University Press, 2010.
- [17] David Pfau, James S Spencer, Alexander GDG Matthews, and William Matthew C Foulkes, ‘Ab-initio solution of the many-electron schrödinger equation with deep neural networks’, *Physical Review Research*, **2**(3), 033429, (2020).
- [18] Maziar Raissi, Paris Perdikaris, and George E Karniadakis, ‘Physics-informed neural networks: A deep learning framework for solving forward and inverse problems involving nonlinear partial differential equations’, *Journal of Computational Physics*, **378**, 686–707, (2019).
- [19] Subir Sachdev, *Quantum Phase Transitions*, Cambridge University Press, 2011.
- [20] Kristof T Schütt, Huziel E Sauceda, Pieter-Jan Kindermans, Alexandre Tkatchenko, and Klaus-Robert Müller, ‘SchNet—a deep learning architecture for molecules and materials’, *The Journal of Chemical Physics*, **148**(24), 241722, (2018).
- [21] E. M. Stoudenmire and D. J. Schwab, ‘Supervised learning with tensor networks’, *Advances in Neural Information Processing Systems*, **29**, 4799–4807, (2016).
- [22] E Miles Stoudenmire and David J Schwab, ‘Supervised learning with quantum-inspired tensor networks’, *Advances in Neural Information Processing Systems*, **29**, (2016).
- [23] Matthias Troyer and Uwe-Jens Wiese, ‘Computational complexity and fundamental limitations to fermionic quantum monte carlo simulations’, *Physical Review Letters*, **94**(17), 170201, (2005).
- [24] Oliver T Unke, Stefan Chmiela, Huziel E Sauceda, Michael Gastegger, Igor Poltavsky, Kristof T Schütt, Alexandre Tkatchenko, and Klaus-Robert Müller, ‘Machine learning force fields’, *Chemical Reviews*, **121**(16), 10142–10186, (2021).
- [25] Evert PL van Nieuwenburg, Ye-Hua Liu, and Sebastian D Huber, ‘Learning phase transitions by confusion’, *Nature Physics*, **13**(5), 435–439, (2017).
- [26] Guillaume Verdon, Trevor McCourt, Enxhell Luzhnica, Vikash Singh, Stefan Leichenauer, and Jack Hidary, ‘Quantum graph neural networks’, *arXiv preprint arXiv:1909.12264*, (2019).
- [27] Tian Xie and Jeffrey C Grossman, ‘Crystal graph convolutional neural networks for an accurate and interpretable prediction of material properties’, *Physical Review Letters*, **120**(14), 145301, (2018).
- [28] Y. You, T. Chen, and Z. Wang, ‘Graph contrastive learning for quantum circuits’, *arXiv preprint arXiv:2106.05926*, (2021).
- [29] Licheng Zhou, Yiming Cai, Jingwei Liu, Zicheng Wei, Hongcheng Zhang, and Qiang Yang, ‘Graphmae2: A decoding strategy for graph masked autoencoders’, *arXiv preprint arXiv:2210.13366*, (2022).
- [30] Yan Zhu, Yuchen Xu, Feng Yu, Qiang Liu, Shu Wu, and Liang Wang, ‘Graph contrastive learning with augmentations’, *Advances in Neural Information Processing Systems*, **34**, 12834–12846, (2021).

Supplementary Material

Detailed supplementary material is provided in a separate document with the submission. The supplementary material contains in-depth information on:

- Appendix A1: Active Learning Framework for Efficient Quantum Simulation
- Appendix A2: Ablation Studies and Comparative Analysis
- Appendix A3: Quantum Information-Theoretic Foundation
- Appendix A4: Additional Baseline Comparison Considerations
- Appendix A5: Additional Limitations and Future Work
- Appendix A6: Out-of-Distribution Transfer Evaluation
- Appendix A7: Tensor Network Surrogate Models
- Appendix A8: Detailed Experimental Setup
- Appendix A9: Additional Conclusion Material

The supplementary material extends and supports the findings presented in this paper without containing any essential information required to understand the main results.